

Bone fracture detection using electrical impedance tomography based on STEMLab Red Pitaya

Khusnul Ain^{1,2}, Osmalina Nur Rahma^{1,2}, Alfian Pramudita Putra^{1,2}, Nur Syavinas¹, Dudi Darmawan³, Harsh Sohal⁴

¹Biomedical Engineering, Faculty of Science and Technology, Universitas Airlangga, Surabaya, Indonesia

²Biomedical Signals and Systems Research Group, Faculty of Science and Technology, Universitas Airlangga, Surabaya, Indonesia

³Department of Engineering Physics, Telkom University, Bandung, Indonesia

⁴Department of Electronics and Communication Engineering, Jaypee University of Information Technology Waknaghat, Himachal Pradesh, India

Article Info

Article history:

Received Apr 11, 2023

Revised Jul 7, 2023

Accepted Jul 16, 2023

Keywords:

Biomeasurement

Bone fracture detection

Electrical impedance

tomography

Healthcare

STEMlab Red Pitaya

ABSTRACT

Bone fractures can result in accidents, osteoporosis, bone cancer, or other conditions. X-Ray is a medical imaging technique often used to detect bone fractures. However, X-Rays can have radiation effects that harm patients, health workers, and the environment. Electrical impedance tomography (EIT) is a system that can obtain object images based on the electrical impedance distribution. In bone fractures, the proximal bone tissue experiences increased blood flow with local edema due to the inflammatory reaction which indicates the presence of a high conductivity diffusion material at the fracture location. EIT based on the STEMLab Red Pitaya module can be utilized to detect bone fractures. Red Pitaya serves as a controller, possessing a voltage generator, an oscilloscope, and 16 input/output pins that fulfill most of the EIT functions. To test the EIT-based system's efficacy, a 3D-printed polylactic acid (PLA)-based bone phantom model was used. This model was placed on a cylindrical phantom filled with water as a substitute for soft tissue. The voltage data then are reconstructed using electrical impedance and diffuse optical reconstruction software (EIDORS), a MATLAB toolbox devoted to image reconstruction from impedance measurement results. The results of the reconstruction demonstrated that EIT based on the Red Pitaya STEMLab module could distinguish between normal bone and fractured bone.

This is an open access article under the [CC BY-SA](https://creativecommons.org/licenses/by-sa/4.0/) license.



Corresponding Author:

Alfian Pramudita Putra

Biomedical Engineering Study Program, Faculty of Science and Technology, Universitas Airlangga

Dr. Ir Soekarno Street, C Campus, Surabaya 60115, Indonesia

Email: alfian.pramudita@fst.unair.ac.id

1. INTRODUCTION

Bone is a vital organ that plays a critical role in enabling various activities. When the bone's function is disrupted, it hinders movements. A fracture is a state of discontinuity in the bone that can result from partial or total trauma [1]. Fractures can be caused by accidents, osteoporosis, bone cancer, or other cases that exert pressure on the bones [2]. Bone fractures are the second most common injury worldwide, affecting 436 million people [3]. According to the World Health Organization (WHO), more than 5.3 million accidents occurred in 2011, 1.3 million of them resulting in bone fractures. 178 million new fracture cases were reported in 2019 worldwide. Besides that, 455 million acute or long-term symptoms of fracture cases were also reported in the same year [4].

Medical devices that are used to detect and diagnose bone fractures are radiography or X-ray tomography (X-ray computerized tomography) [5]–[8], magnetic resonance imaging (MRI) [9]–[11], and ultrasonography (USG) [12]. However, these instruments have several weaknesses, such as high cost and negative effects on the body [13]. The medical imaging tool that is widely used for detecting bone fractures is X-ray since it is the fastest and the easiest due to its speed and ease of use. However, X-ray has some drawbacks, such as radiation effects that can harm the patients, health workers, and hospital environment. Regular use of X-rays is harmful to the body since it can cause hematopoietic disorders (blood disorders) like anemia, leukemia, and leukopenia. It can also kill cells in the body and increase the probability of cancer [14].

Electrical impedance tomography (EIT) is an electrical-based imaging technique that can image body tissues [15] by mapping the distribution of electrical impedance in each tissue [16]. The tissue impedance values are obtained from the characteristics of biological tissue that inhibit electrical currents injected into the body. Human tissue has varying electrical conductivity values, ranging from 15.4 mS/cm for cerebrospinal fluid to 0.06 mS/cm for bone [15]. These conductivity differences result in a different impedance value. Therefore, the electrical impedance method can be applied to EIT to obtain image reconstruction of human tissue [15]. EIT can detect tissue abnormalities due to differences in tissue impedance. EIT assesses the internal characteristics of the human body by injecting an electric current through electrodes mounted on its surface [17]. Bone tissue has significant bioelectrical variation because of its morphological diversity. In fractures, the proximal bone tissue experiences increased blood flow with local edema due to the inflammatory reaction and the bone's healing process. These events indicate the presence of material diffusion with low electrical resistance in the fractured part [18], [19].

EIT has been widely used in the medical field, including the treatment of the thorax, to detect lung function, abnormalities in the respiratory system, breast cancer, heart function, and brain nerves [20]. The advantages of EIT are that the device is portable and non-invasive so patients feel comfortable during examinations, and there is minimal risk of harm. EIT does not cause long-term risks when compared to MRI, computed tomography (CT), and X-ray [21]. Research related to portable EIT has been conducted by building a STEMLab Red Pitaya-based system at an affordable cost [22]. The system was tested on eggs with different heating times using eight electrodes [23]. The STEMLab Red Pitaya can fully utilize hardware control, signal generation, and data acquisition capabilities to implement most EIT functions. The EIT system developed based on STEMLab Red Pitaya can measure biological tissue with high accuracy at an economical cost.

Based on the problems described, a portable EIT system based on the Red Pitaya STEMLab module can be designed to detect bone fractures. The Red Pitaya was used as a controller because it has a function generator as a voltage generator, an oscilloscope as a signal reader, and 16 input/output pins as channel controllers, allowing it to perform most of the EIT functions. This study used a phantom made of 3D-printed PLA to substitute bone placed in a water cylinder for soft tissue. The phantoms used were divided into two types: phantoms with normal bone conditions and those with fractures. The reconstruction software used is electrical impedance and diffuse optical reconstruction software (EIDORS), a MATLAB toolbox dedicated to image reconstruction from impedance measurement results.

2. MATERIALS AND METHODS

2.1. Hardware design

The hardware design of the EIT system is shown in Figure 1. The system consists of data acquisition device STEMLab Red Pitaya, DC Block, buffer circuit, the voltage controlled current source (VCCS), demultiplexer, multiplexer, instrument amplifier, and filter circuit. Demultiplexer has a function to inject current from VCCS to the phantom and multiplexer has a function to measure the voltage originating from the phantom.

2.2. STEMLab Red Pitaya modul driver

The STEMLab Red Pitaya 125-14 ultimate kit module has two oscilloscope inputs and two function generator outputs with a sample rate of 125 Msps each and a bandwidth of 50 MHz. The module is also equipped with memory to store data. The STEMLab Red Pitaya module has 16 digital input/output pins and supply voltages of +3.3 Volts, -3.3 Volts, and 5 Volts. The STEMLab Red Pitaya module was chosen for its ability to fulfill most of the functions of EIT. It can generate an alternating current (AC) voltage signal and act as both a function generator and oscilloscope due to its digital analog converter (DAC) and analog digital converter (ADC). The DAC converts the digital signal sent by the PC into an analog signal that the voltage controlled current source (VCCS) can read, while the ADC converts the measured voltage signal into a digital signal that a personal computer (PC) can recognize. The STEMLab Red Pitaya module can also control demultiplexers and multiplexers to manage current injection, provide grounding, or measure voltage. The signal acquisition process using the Red Pitaya STEMLab module begins by measuring the voltage signal,

which is sent to Red Pitaya. The voltage signal then passes through a low-pass filter and the ADC converts the signal to fill the data buffer on the field programmable gate arrays (FPGA).

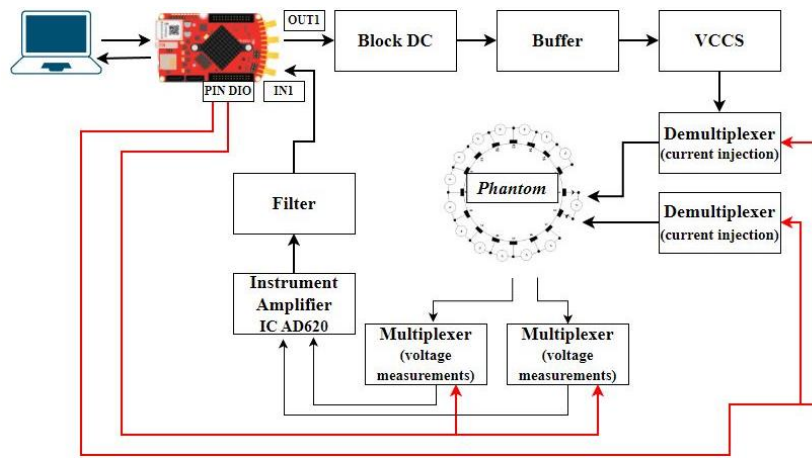


Figure 1. Block diagram of EIT based on STEMLab Red Pitaya

2.3. Software design

The MATLAB software was utilized to control the STEMLab Red Pitaya module, which generates AC voltage signals, performed ADC and DAC conversions, and carried out the filtering process. Additionally, it controlled the demultiplexer for current injection, managed the multiplexer for voltage measurement, and handled data acquisition and grouping. Matlab is a data analysis program that supports standard commands for programmable instruments (SCPI) commands to retrieve data stored in the Red Pitaya STEMLab Module. To connect the STEMLab Red Pitaya module with MATLAB, one needs the IP address of the module, which is available on the Red Pitaya web browser.

The processing was initiated by connecting the USB cable from the STEMLab Red Pitaya module to the laptop and the universal serial bus (USB) power module to the STEMLab Red Pitaya socket. Then, the code provided was entered to access the Red Pitaya web. Once the web is opened, enter the SCPI server section, click the run button, and the internet protocol (IP) address of the STEMLab Red Pitaya module being used would appear. By entering this IP address into the Matlab program code, one can connect the STEMLab Red Pitaya module with Matlab so that it can execute commands from the Matlab program. Next, one needed to write program code in Matlab to generate an AC voltage signal and controlled the work process from STEMLab Red Pitaya to build an EIT system. Image reconstruction was performed with EIDORS-V3.10. This software performed the image reconstruction of measurement data on EIT. The result was a tomographic image that show the difference in electrical impedance.

2.4. Bone phantom design

The EIT system for detecting bone fractures was tested on artificial bone phantoms in aqueous media, which were used as a substitute for soft tissue. The phantoms were designed to resemble the femur bone and were 3D printed using polylactic acid (PLA). PLA was selected for its availability and suitability for 3D printing. Two types of bone phantoms were used in the experiment: normal and fractured bone. Sixteen electrodes were then placed around the phantom, with a width of 15 mm and a height of 30 mm. The electrodes were connected to both the current-injecting demultiplexer and the voltage-measuring multiplexer.

2.5. Data analysis

During the data analysis process, the image reconstruction results of the normal femur bone and fractured femur bone were compared against the axial images of 3D printing objects, as shown in Figure 2. Figure 2(a) showed the transversal section of the phantom in an aqueous chamber with normal bone in an acrylic tube as the environment while Figure 2(b) depicted the fractured bone in an acrylic tube. Each tissue has a different impedance value; also, with impedance values, it can detect physiological changes in the tissue. So, the area will have an additional impedance value when a fracture occurs in the bone. The impedance difference can be observed by the color differences in the reconstructed image. Different colors identify different tissue types and can detect physiological changes in tissues. EIDORS software uses a color scheme

to represent different tissue types, with dark blue, light blue, white, yellow, red, and maroon representing different impedance values. If an object has a lower impedance value than other objects, then the object will be represented in dark blue; the higher the object's impedance value, the brighter the color will be. Meanwhile, objects with zero impedance values are represented in white.

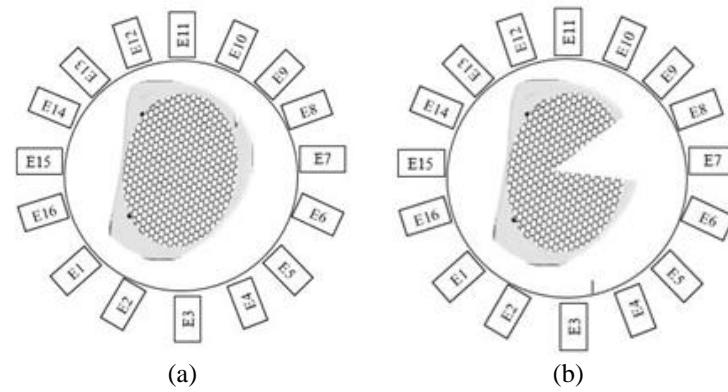


Figure 2. Transversal section of the phantom in an aqueous chamber (a) normal bone in an acrylic tube and (b) fractured bone in an acrylic tube

3. RESULTS AND DISCUSSION

3.1. EIT modul systems

The EIT system requires generator, VCCS, and band pass filter modules which must be made and tested for performance before being installed as a single EIT system unit. Red pitaya's ability to produce a signal generator was tested by connecting the OUT1 extension connector (pin in the STEMLab Red Pitaya module as shown in Figure 1 to an oscilloscope with a sampling frequency variation from 100 Hz to 4 MHz. The Vrms to frequency is shown in Figure 3.

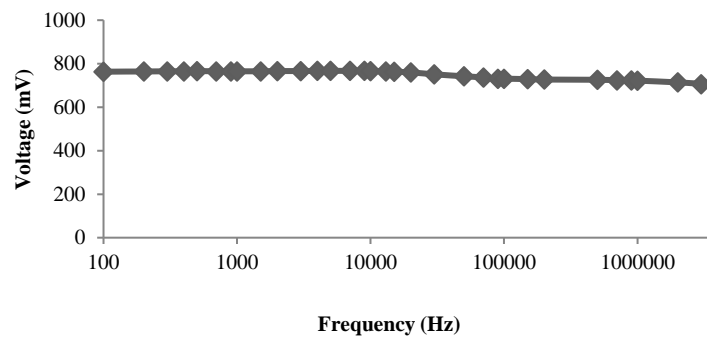


Figure 3. Vrms of generated signals from Red Pitaya

Figure 3 shows that the Red Pitaya device can serve as a signal generator, producing sine signals from 0 Hz to 1 MHz. Given that the collected data's frequency was 10 kHz, the Red Pitaya is suitable to be utilized as a generator in the EIT system. The Vrms of the signals in several frequencies are stable and the signal frequency of data collection was also included in that frequency.

VCCS is a current source that controls the incoming voltage to produce a constant and stable current value. The VCCS circuit is built with OPA2134 components and four 1kΩ resistors. The VCCS test determines how consistent the current coming out of the circuit is to withstand a given load. The VCCS circuit used the OPA2134, a dual op-amp IC where one op-amp was used as a buffer circuit, and the other op-amp was used as a VCCS circuit. The resulting VCCS capability has the characteristics shown in Figure 4. The test results for the VCCS circuit are shown in Figure 4. Loading of 100 Ω to 1 kΩ at a frequency of 10 kHz produced a constant current of 0.78 mA, but a drastic decrease occurred when a frequency of 1 MHz was applied. The EIT system is equipped with a bandpass filter to pass bandpasses within a specified limit range to improve data

quality. Theoretically, this bandpass filter circuit has a cut-off frequency value of 1.59 Hz to 159 kHz. The characteristics of the resulting bandpass filter are shown in Figure 5.

The test results of the signal had a stable output voltage in the frequency range of 5 Hz to 50 kHz, which did not match the theoretical calculations; this was due to the tolerance values of the resistors and capacitors used, which caused the test results to deviate from the desired expectations. However, the frequency range still fell within the frequency range used in the EIT system, which is 10 kHz.

During the testing of the AD620 amplifier, variations in gain and frequency resulted in discrepancies between the output voltage measured using an oscilloscope, and the calculated results from the system. However, by adding a 10 k Ω resistor on the RG IC AD620 pin, a significant gain of 5.94 was achieved. This value was chosen because the test results for this gain produced a consistent and stable measurement that matched the calculated results, unlike other gain values that produced inconsistent measurements.

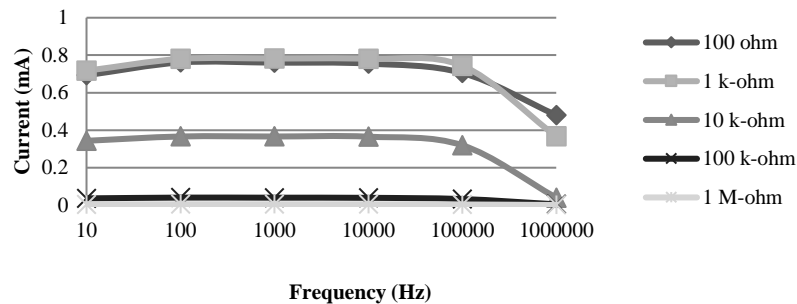


Figure 4. Characteristics of the resulting VCCS capability

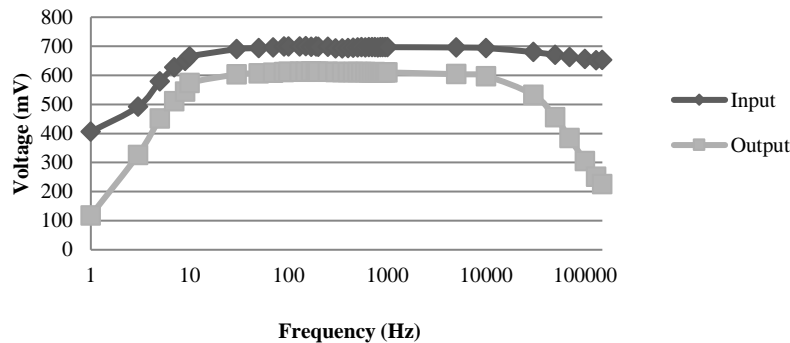


Figure 5. Characteristics of the resulting bandpass filter

3.2. Phantom making

The Phantom was composed of 3D printed bone from PLA with a bone height of 22 cm, a weight of 2.5 grams, and a diameter of 12 mm, which was placed in an acrylic tube 20 cm high and 5.8 cm in diameter with 16 electrodes inside as shown in Figure 6. Figure 6(a) shows a regular and a fractured bone phantom made of PLA by using 3D printing method, while Figure 6(b) shows the acrylic tube which was used as the chamber to do the measurement the impedance and electrodes to supply current to the phantom. The phantom was designed to represent the actual object, bone encased in flesh.

3.3. Data acquisition

Once each component has been tested, they were assembled into a single unit on a printed circuit board (PCB). Overall testing of the device was carried out by taking data from the phantom that had been made. The device started by generating a generator signal on the Red Pitaya. Then, the AC signal went to VCCS, which controlled the input voltage so that the current coming out of the circuit was constant. After that, the current from VCCS was sent to the multiplexer to be injected into the phantom electrode. The current injection process was carried out sequentially from the 1st to the 16th electrode. The voltage was also measured at two adjacent electrodes when the current injection process occurred.

The result of the voltage value measured by the two adjacent electrodes was then inputted into the amplifier instrument on the positive input and negative input legs. The signal input on the AD620 IC was reduced between the positive input and the negative input, and the reduction was amplified by 5.94x due to the resistor value installed on the RG pin. This amplified the voltage signal coming out of the AD620 to a single voltage signal. After amplification, the signal was filtered through a bandpass filter to remove noise. The final results of the measurement data were then re-acquired by Red Pitaya and stored in the PC folder for reconstruction later.

Data collection was carried out using the neighboring method. In this method, a current I was applied to a pair of adjacent electrodes on the phantom, and then the voltage V was measured on each set of adjacent electrodes alternately. After the surrounding voltage was measured, the current would move to the next pair of electrodes; this process continued until 256 voltage measurement data were obtained [24]. Figure 7 shows the EIT device during data collection.

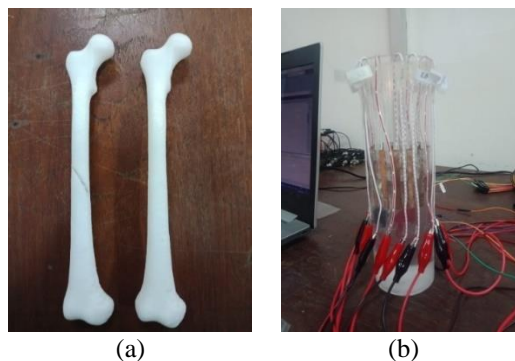


Figure 6. The bone phantom and its configuration for EIT (a) 3D printing of fractured and normal bones and (b) Acrylic tube and electrodes configuration

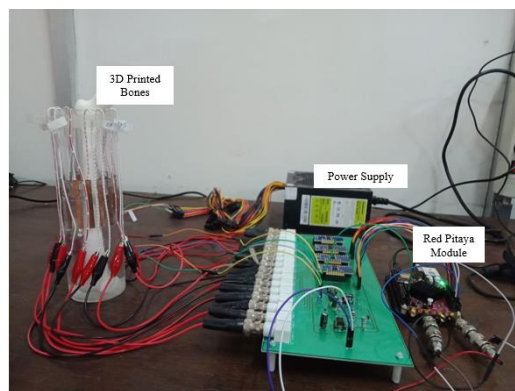


Figure 7. The data acquisition in EIT System

Data collection was carried out by filling the tube with water as high as 11 cm so the copper plate electrode was submerged. Then water data was collected for a frequency of 10 kHz. Figure 8 shows phantom data containing pure water, a normal bone in water, and a fractured bone in water at a frequency of 10 kHz.

Based on Figure 8, it can be observed that there are only minor differences in the data. Water data were used as reference data to solve the finite element model by assuming water has homogeneous conductivity and then calculating the water stress distribution [24]. The stress data resulting from 3D printing of normal bone and fracture objects were entered into the program alternately and then solved with the inverse problem. This process subtracted the water data from the 3D printed bone data so 3D printed bone and fracture conductivity distribution images were produced. By analyzing the data difference between normal bone and the fractured one, the fracture was detected. The color index on EIDORS showed the conductivity distribution from high to low, with blue indicating low conductivity and red indicating high conductivity [25].

Conductivity refers to the ability of a material to conduct electric current and is related to the substance contained in the material. PLA is a polymer made from lactic acid that can be used as a conventional plastic

material. Because the test material used in this study was made from 3D printing bone from PLA, this material has a slight ability to conduct electric current, resulting in a small conductivity value.

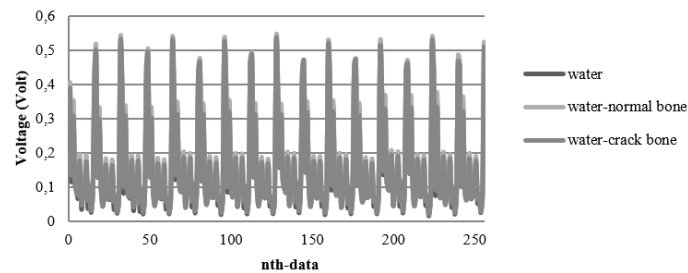


Figure 8. The potential difference from water, 3D Bone in water, and 3D bone fracture in water at 10 kHz

3.4. Image reconstruction

The reconstruction was carried out with EIDORS software using a relative imaging method called one-step Gaussian Newton [26]. To use this method, a hyperparameter value is needed to minimize image noise and ensure adequate visualization of objects. In this study, a value of 0.001 was used. Water scan data served as reference data, while 3D printing data of normal bone and fracture bone were used as object data. Relative imaging techniques reduce the reference data to object data so that a reconstructed image is produced close to the reference object, between reference data and object data, using the same frequency, 10 kHz. Figure 9 shows the reconstructed images from 3D printing: i) a normal bone, ii) a 3D printing reconstruction image of a fractured bone, and iii) an image of only the fracture reconstruction.

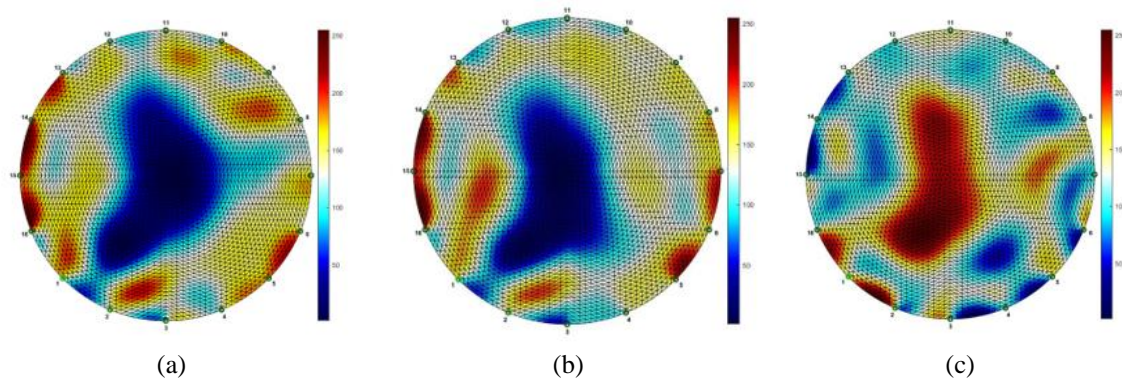


Figure 9. Comparison of image reconstruction results (a) 3D printed normal bone at 10 kHz, (b) 3D-printed fractured bone at 10 kHz, and (c) Only 3D-printed fractured bone section at 10 kHz

Based on the results of the image reconstruction obtained, as shown in Figures 9(a)-9(c), it is evident that a blue area in the middle indicates a smaller conductivity distribution value than the surrounding areas, which are represented in yellow to red in the color index, indicating a more significant value. The color index reflects the conductivity distribution. The phantom 3D printing of normal bones and fractures as a result of reconstruction using EIDORS is represented in blue, indicating a smaller conductivity distribution than the surrounding aqueous media with a higher conductivity distribution represented in yellow to red. The yellow to red is noise from the measurement results, which can be caused by electrodes that are too small in the distance and can also be caused by the possibility of other substances being mixed with water.

When reconstructing 3D-printed normal or fractured bone phantom using water reference data, both exhibit the same conductivity range, indicated by blue Figures 9(a) and 9(b). The difference can be observed based on the area of reconstruction as shown in Figure 10. The normal bone has an area of 3,132 pixels as shown in Figure 10(a). In comparison, 3D reconstruction of imagery fracture bone has a size of 2,735 pixels, as shown in Figure 10(b). Area measurements were performed using ImageJ software.

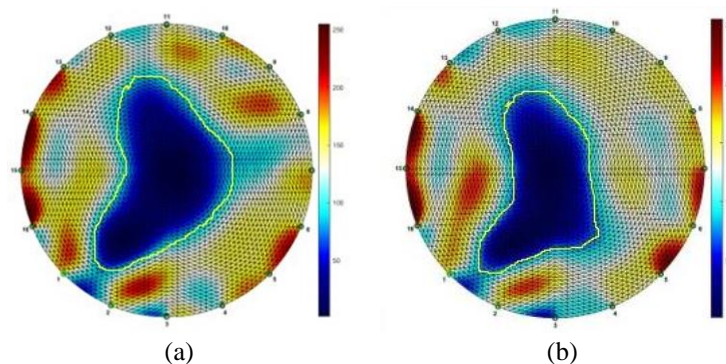


Figure 10. The image reconstruction area of (a) 3D-printed normal bone, (b) 3D-printed fractured bone

Based on the results of the image reconstruction carried out, it can be seen that the EIT built in this study was capable of detecting differences between 3D printing of normal bone and fractures using a frequency of 10 kHz. This result was from the previous study, which also used a frequency of 10 kHz [27]. Apart from that, when the 3D printing of normal bones was reconstructed with the 3D printing of fractured bones, it appeared that there was only part of the fracture. This result is also suitable with the previous studies which investigated how to detect bone cancer [28] and plate composite [29]. For future exploration, it is better to use bovine natural bone as a phantom or use a 3D printed-bone phantom but originating from bone-like materials, such hydroxyapatite or β -tricalcium phosphate so that it can represent natural bone [30], [31].

4. CONCLUSION

The STEMLab Red Pitaya 125-14 module can be fully utilized to build an EIT system that works by generating a signal generator, controlling the current injection process via the multiplexer, adjusting the voltage measurement on two adjacent electrodes by the demultiplexer, and carrying out measurement data acquisition. In this case, the pressure at the object being measured is in 3D printing of normal bone and fracture. The results of image reconstruction using the EIDORS software from the EIT system have been made to distinguish between normal and fractured bone. The 3D printing image reconstruction of normal bones and fractures has a small conductivity, so it appears in blue in EIDORS. Additionally, the results of image reconstruction between 3D printing bones and fractures have different shapes, with the best imaging results obtained at a frequency of 10 kHz to distinguish between the two.

ACKNOWLEDGEMENTS

The authors thank the Faculty of Science and Technology, Universitas Airlangga, for funding this research under Excellence Faculty Research with grant Number 251/UN3/2022.

REFERENCES

- [1] A. Bigham-Sadegh and A. Oryan, "Basic concepts regarding fracture healing and the current options and future directions in managing bone fractures," *International Wound Journal*, vol. 12, no. 3, pp. 238–247, Jun. 2015, doi: 10.1111/iwj.12231.
- [2] O. Bandyopadhyay, A. Biswas, and B. B. Bhattacharya, "Long-bone fracture detection in digital X-ray images based on digital-geometric techniques," *Computer Methods and Programs in Biomedicine*, vol. 123, pp. 2–14, 2016, doi: 10.1016/j.cmpb.2015.09.013.
- [3] A. Cieza, K. Causey, K. Kamenov, S. W. Hanson, S. Chatterji, and T. Vos, "Global estimates of the need for rehabilitation based on the Global Burden of Disease study 2019: a systematic analysis for the Global Burden of Disease Study 2019," *The Lancet*, vol. 396, no. 10267, pp. 2006–2017, Dec. 2020, doi: 10.1016/S0140-6736(20)32340-0.
- [4] A. M. Wu *et al.*, "Global, regional, and national burden of bone fractures in 204 countries and territories, 1990–2019: a systematic analysis from the Global Burden of Disease Study 2019," *The Lancet Healthy Longevity*, vol. 2, no. 9, pp. e580–e592, Sep. 2021, doi: 10.1016/S2666-7568(21)00172-0.
- [5] P. Augat, E. F. Morgan, T. J. Lujan, T. J. MacGillivray, and W. H. Cheung, "Imaging techniques for the assessment of fracture repair," *Injury*, vol. 45, no. SUPPL. 2, pp. S16–S22, Jun. 2014, doi: 10.1016/j.injury.2014.04.004.
- [6] Y. Cao, H. Wang, M. Moradi, P. Prasanna, and T. F. Syeda-Mahmood, "Fracture detection in x-ray images through stacked random forests feature fusion," in *2015 IEEE 12th International Symposium on Biomedical Imaging (ISBI)*, Apr. 2015, vol. 2015-July, pp. 801–805, doi: 10.1109/ISBI.2015.7163993.
- [7] N. Umadevi and S. N. Geethalakshmi, "Multiple classification system for fracture detection in human bone x-ray images," in *2012 Third International Conference on Computing, Communication and Networking Technologies (ICCCNT'12)*, Jul. 2012, pp. 1–8, doi: 10.1109/ICCCNT.2012.6395889.

- [8] W. Zheng and L. Zhang, "Study on recognition of the fracture injure site based on X-ray images," in *Proceedings - 2010 3rd International Congress on Image and Signal Processing, CISP 2010*, Oct. 2010, vol. 4, pp. 1947–1950, doi: 10.1109/CISP.2010.5648055.
- [9] M. P. Brady and W. Weiss, "Clinical Diagnostic Tests Versus MRI Diagnosis of ACL Tears," *Journal of Sport Rehabilitation*, vol. 27, no. 6, pp. 596–600, Nov. 2018, doi: 10.1123/jsr.2016-0188.
- [10] J. A. Clavero *et al.*, "MR imaging of ligament and tendon injuries of the fingers," *Radiographics*, vol. 22, no. 2, pp. 237–256, Mar. 2002, doi: 10.1148/radiographics.22.2.g02mr11237.
- [11] W. Mallee, J. N. Doornberg, D. Ring, C. N. Van Dijk, M. Maas, and J. C. Goslings, "Comparison of CT and MRI for diagnosis of suspected scaphoid fractures," *Journal of Bone and Joint Surgery*, vol. 93, no. 1, pp. 20–28, Jan. 2011, doi: 10.2106/JBJS.I.01523.
- [12] H. C. Bäcker, C. H. Wu, and R. J. Strauch, "Systematic review of diagnosis of clinically suspected scaphoid fractures," *Journal of Wrist Surgery*, vol. 09, no. 01, pp. 081–089, 2020, doi: 10.1055/s-0039-1693147.
- [13] M. S. Beck and R. A. Williams, "Process tomography: a European innovation and its applications," *Measurement Science and Technology*, vol. 7, no. 3, pp. 215–224, Mar. 1996, doi: 10.1088/0957-0233/7/3/002.
- [14] Z. Zhekova-Maradzhieva *et al.*, "The effect of X-ray radiation on the human body - pros and cons. Radiation protection in medical imaging and radiotherapy," *Scripta Scientifica Salutis Publicae*, vol. 2, no. 0, p. 161, Jan. 2017, doi: 10.14748/sssp.v2i0.4037.
- [15] J. D. Bronzino, *The biomedical engineering handbook*, 2nd ed. Boca Raton: CRC Press LLC, 2006.
- [16] A. Adler and A. Boyle, "Electrical impedance tomography: Tissue properties to image measures," *IEEE Transactions on Biomedical Engineering*, vol. 64, no. 11, pp. 2494–2504, 2017, doi: 10.1109/TBME.2017.2728323.
- [17] J. P. Leitzke and H. Zangl, "A review on electrical impedance tomography spectroscopy," *Sensors (Switzerland)*, vol. 20, no. 18, pp. 1–19, 2020, doi: 10.3390/s20185160.
- [18] A. H. Dell'osa, C. J. Felice, and F. Simini, "Bioimpedance and bone fracture detection: A state of the art," *Journal of Physics: Conference Series*, vol. 1272, no. 1, 2019, doi: 10.1088/1742-6596/1272/1/012010.
- [19] A. H. Dell'osa, A. Concu, F. Dobarro, and J. C. Felice, "Bone fracture detection by electrical bioimpedance: measurements in ex vivo mammalian femur," *IFMBE Proceedings*, vol. 72, pp. 203–207, 2020, doi: 10.1007/978-981-13-3498-6_30.
- [20] I. Sapuan, M. Yasin, K. Ain, and R. Apsari, "Anomaly detection using electric impedance tomography based on real and imaginary images," *Sensors*, vol. 20, no. 7, p. 1907, Mar. 2020, doi: 10.3390/s20071907.
- [21] T. A. Khan and S. H. Ling, "Review on electrical impedance tomography: artificial intelligence methods and its applications," *Algorithms*, vol. 12, no. 5, p. 88, Apr. 2019, doi: 10.3390/a12050088.
- [22] H. Chen *et al.*, "Development of a portable electrical impedance tomography device for online thrombus detection in extracorporeal-circulation equipment," *IEEE Sensors Journal*, vol. 21, no. 3, pp. 3653–3659, Feb. 2021, doi: 10.1109/JSEN.2020.3022078.
- [23] Z. Xu *et al.*, "Development of a portable electrical impedance tomography system for biomedical applications," *IEEE Sensors Journal*, vol. 18, no. 19, pp. 8117–8124, 2018, doi: 10.1109/JSEN.2018.2864539.
- [24] M. T. Erwati and N. Farrukh, "Application of electrical impedance tomography for imaging in bio-medical and material technology," in *2009 IEEE Student Conference on Research and Development (SCOREd)*, 2009, pp. 168–171, doi: 10.1109/SCOREd.2009.5443175.
- [25] V. Sarode, P. M. Chimurkar, and A. N. Cheeran, "Electrical impedance tomography using EIDORS in a closed phantom," *International Journal of Computer Applications*, vol. 48, no. 19, pp. 48–52, Jun. 2012, doi: 10.5120/7460-0526.
- [26] A. Widodo and Endarko, "Experimental study of one step linear Gauss-Newton algorithm for improving the quality of image reconstruction in high-speed Electrical Impedance Tomography (EIT)," *Journal of Physics: Conference Series*, vol. 1120, no. 1, p. 012067, Nov. 2018, doi: 10.1088/1742-6596/1120/1/012067.
- [27] Z. Kamus, A. Nofrianto, Y. W. Satwika, E. Ekawati, and D. Kurniadi, "Optimization of object injection current in the development of electrical impedance tomography for bone fracture detection," *Journal of Physics: Conference Series*, vol. 2309, no. 1, 2022, doi: 10.1088/1742-6596/2309/1/012034.
- [28] N. Saha and M. A. Rahaman, "Bone cancer detection using electrical impedance tomography," *Indonesian Journal of Electrical Engineering and Computer Science*, vol. 24, no. 1, p. 245, Oct. 2021, doi: 10.11591/ijeecs.v24.i1.pp245-252.
- [29] J. Tanabalou and R. Priyadarshini, "Smart monitoring system of composite plates for structural health monitoring using electromechanical impedance approach," *Indonesian Journal of Electrical Engineering and Computer Science*, vol. 25, no. 3, p. 1375, Mar. 2022, doi: 10.11591/ijeecs.v25.i3.pp1375-1382.
- [30] A. S. Budiati *et al.*, "Exploration of bovine bone waste as source of bovine hydroxyapatite synthesis and its composite with gelatin-hydroxypropylmethyl cellulose as injectable bone substitute," *Ecology, Environment and Conservation*, vol. 26, pp. S135–S140, 2020.
- [31] A. P. Putra, I. Faradisa, D. Hikmawati, and Siswanto, "The effect of Hydroxyapatite-gelatin composite with Alendronate as Injectable Bone Substitute on Various Hydroxyapatite-Based Substrate," *2019 International Biomedical Instrumentation and Technology Conference, IBITeC 2019*, pp. 41–45, 2019, doi: 10.1109/IBITeC46597.2019.9091686.

BIOGRAPHIES OF AUTHORS



Khusnul Ain    received the S.T. degree in nuclear engineering from Gadjah Mada University, Indonesia, in 1995, an M.Si. degree in Physical Sciences from Gadjah Mada University, Indonesia, in 2002, and a Doctoral degree in Engineering Physics from Bandung Institute of Technology, Indonesia, in 2014. Currently, he is a senior lecturer at the Biomedical Engineering Study Program, Department of Physics, Faculty of Science of Technology, Universitas Airlangga, Indonesia. His research interests include biomeasurement, electrical impedance, computational modeling, and bioinstrumentation. He can be contacted at email: k_ain@fst.unair.ac.id.



Osmalina Nur Rahma    received the S.T. degree in biomedical engineering from Universitas Airlangga, Indonesia, in 2013 and the M.Si. degree in biomedical engineering from the University of Indonesia, Indonesia, in 2016. Currently, she is a lecturer at the Biomedical Engineering Study Program, the Department of Physics, Faculty of Science of Technology, Universitas Airlangga, Indonesia. Her research interests include biomedical instrumentation, signal processing, and rehabilitation engineering. She can be contacted at email: osmalina.n.rahma@fst.unair.ac.id.



Alfian Pramudita Putra    received the S.T. degree in biomedical engineering from Universitas Airlangga, Indonesia, in 2014 and the M.Sc. degree in biomedical engineering from the University of Groningen, The Netherlands, in 2017. Currently, he is a lecturer at the Biomedical Engineering Study Program, Department of Physics, Faculty of Science of Technology, Universitas Airlangga, Indonesia. His research interests include biomechanics, biomedical instrumentation, rehabilitation engineering, biomedical signal processing, and biomedical product development. He can be contacted at email: alfian.pramudita@fst.unair.ac.id.



Nur Syavinas    received the S.T. degree in biomedical engineering from Universitas Airlangga, Indonesia in 2022. Her research interests include biomedical instrumentation and biomeasurement. She can be contacted at email: nur.syavinas-2018@fst.unair.ac.id.



Dudi Darmawan    completed his undergraduate program in instrumentation physics, a master's degree in instrumentation and control, and finally, his doctorate in physical engineering at the Bandung Institute of Technology in 2015. The research field when completing his doctoral program is in the field of tomography, and research still being conducted up to now is about non-destructive testing. Currently, he has worked as a lecturer at Telkom University since 1999. He can be contacted at email: dudidw@telkomuniversity.ac.id.



Harsh Sohal    received B. Tech. Degree in Electronics and Instrumentation Engineering from Punjab Technical University Jalandhar, Punjab, India in 2005 and M. Tech. degree in VLSI Design from the National Institute of Technology Hamirpur, India, in 2008. He completed his Ph.D. in Biomedical Engineering from Kyung Hee University, South Korea, in 2014. Currently, he is working as an Associate Professor in the Department of Electronics and Communication Engineering at the Jaypee University of Information Technology Wanknaghat, Himachal Pradesh, India. He is a member of IEEE and a life member of the biomedical engineering society of India. His research plans include application-specific implementation of various algorithms and VLSI digital signal processing catering to applications in biomedical engineering. He can be contacted at email: harsh.sohal@juit.ac.in; harshsohal@gmail.com